



# Determination of fatty acid and sphingoid base composition of eleven ceramide subclasses in *stratum corneum* by UHPLC/scheduled-MRM

Gilbert P. Laffet<sup>1</sup> · Alexandre Genette<sup>1</sup> · Bastien Gamboa<sup>1</sup> · Virginie Auroy<sup>2</sup> · Johannes J. Voegel<sup>1</sup>

Received: 10 January 2018 / Accepted: 2 May 2018 / Published online: 9 May 2018  
© Springer Science+Business Media, LLC, part of Springer Nature 2018

## Abstract

**Introduction** Ceramides play a key role in skin barrier function in homeostatic and pathological conditions and can be sampled non-invasively through *stratum corneum* collection.

**Objectives** To develop a novel UHPLC/Scheduled MRM method for the identification and relative distribution of eleven classes of ceramides, which are separated by UHPLC and determined by their specific retention times. The precise composition of the fatty acid and sphingoid base parts of each individual ceramide is determined via mass fragmentation.

**Methods** More than 1000 human and pig ceramides were identified. Three human and minipig ceramide classes, CER[AS], CER[NS] and CER[EOS] have been investigated in depth.

**Results** Sphingoid bases were characterized by a prevalence of chain lengths with sizes from C16 to C22, whereas fatty acids were mainly observed in the range of C22–C26. Overall, the ceramide profiles between human and minipig *stratum corneum* were similar. Differences in the CER[AS] and CER[NS] classes included a more homogeneous distribution of fatty acids (16–30 carbon atoms) in minipig, whereas in human longer fatty acid chains (> 24 carbon atoms) predominated.

**Conclusion** The method will be useful for the analysis of healthy and pathological skin in various species, and the measurement of the relative distribution of ceramides as biomarkers for pharmacodynamic studies.

**Keywords** Ceramides · *Stratum corneum* · Non-invasive sampling · UHPLC/scheduled-MRM · Sphingoid bases · Fatty acids

## 1 Introduction

The *stratum corneum* (SC) is the outermost layer of skin and the main barrier against transepidermal water and electrolyte loss. It protects the organism from toxic compounds, allergens and penetration of pathogenic microorganisms (Jungersted et al. 2008; Hinder et al. 2011; Feingold and Elias

2014; Elias 2014; Imokawa et al. 1991; Vietzke et al. 2001). The epidermal barrier function in human *stratum corneum* resides primarily in two compartments, enucleated corneocytes and extracellular lipids, which are often represented by the brick and mortar model. Skin is therefore a tissue highly specialized in the synthesis of lipids. Perturbed lipid metabolism leads to a disturbed skin barrier associated with difficulties in maintaining fluid, electrolyte balance and a higher risk of infection. A relationship between altered SC lipid profiles and impaired skin barrier function has been described in many skin diseases, such as atopic dermatitis (Kezic et al. 2014; Grösch et al. 2012; Elias 2014).

The extracellular lipid matrix is composed of three main lipid classes: Ceramides (CER) form about 40–50% of the lipid content; cholesterol and cholesterol sulphate (CH and CS) form about 25% of lipid content and are involved in desquamation and lipid organization and free fatty acids (FFA) form about 15% of lipid content and are mainly involved in lipid organization (Elias 2014; Feingold and Elias 2014; Janssens et al. 2012).

**Electronic supplementary material** The online version of this article (<https://doi.org/10.1007/s11306-018-1366-4>) contains supplementary material, which is available to authorized users.

✉ Gilbert P. Laffet  
gilbert.laffet@galderma.com

✉ Johannes J. Voegel  
johannes.voegel@galderma.com

<sup>1</sup> Molecular Dermatology, Department of Research, Galderma R&D – Nestlé Skin Health, 2300 Route des Colles, 06902 Sophia Antipolis, France

<sup>2</sup> Albhades Provence, 940 avenue de Traversetolo, 04700 Oraison, France

Contributing to the formation of lamellae structures in the intercellular space, ceramides play a crucial role in lipid organization in SC, cell adhesion and epidermal differentiation (Rabionet et al. 2014).

*Stratum corneum* of human skin contains a complex mix of ceramides consisting of three types of fatty acid moieties known as nonhydroxy [N],  $\alpha$ -hydroxy [A] and ester-linked  $\omega$ -hydroxy [EO] fatty acids. These are bound to four types of sphingoid base moieties, sphingosine [S], dihydrosphingosine [dS], phytosphingosine [P], and 6-hydroxy-sphingosine [H], respectively (Jeroen van Smeden and Bouwstra 2016). Based on the combinatorial connection of fatty acid and sphingoid base structures twelve ceramide classes are formed in human skin. (Ceramide nomenclature and structures are described in Supplemental Table S1).

The chain lengths of fatty acids may vary from 12 up to 30 carbon atoms and, in the sphingoid base, from 16 up to 24 carbon atoms, respectively, creating hundreds of unique molecular structures (Jia et al. 2016; Jeroen; van Smeden and Bouwstra 2016). The long chain omega-esterified ceramides found in SC contain an additional fatty acid, usually a linoleate moiety, attached to the acyl chain and are considered as structural lipids pivotal for the integrity of the epidermal barrier (Janssens et al. 2012; Pilgram et al. 2001).

Recently, additional ceramide classes have been reported in healthy human stratum corneum including 1-*O*-acylceramides and  $\omega$ -hydroxy-ceramides (Janssens et al. 2012; Rabionet et al. 2013).

The analysis of ceramides has been described in the past (Imokawa et al. 1991; Vietzke et al. 2001), and during the last decade, liquid chromatography/mass spectrometry (LC/MS) technologies have become a powerful tool for ceramide analysis. With respect to the LC conditions, mainly normal phase HPLC methods have been described. This limits the degree of flexibility in the choice of the stationary phase. To compensate for the poor separation capacity of normal phase HPLC, high resolution MS detection, like Time Of Flight measurements have been performed (Janssens et al. 2012; Masukawa et al. 2009). With respect to ceramide distribution while, the total number of carbon atoms was reported, no information was provided on the distribution of the chain lengths for the fatty acid and sphingoid base parts, respectively. Another drawback was the necessity to obtain a multitude of difficult to synthesize standards of every ceramide class.

Recently, quantitative methods for the profiling of ceramides have been described using multiple reaction monitoring (MRM) as well as modern UHPLC approaches (Boiten et al. 2016; Jia et al. 2016; Masukawa et al. 2009; t'Kindt et al. 2012). Although around 480 individual ceramide species have been reported, no comprehensive ceramide catalogue, describing the relative abundance of all ceramides, including their precise fatty acid and sphingoid base

structure, has been elaborated (Boiten et al. 2016; Jia et al. 2016; Masukawa et al. 2009; t'Kindt et al. 2012; van Smeden et al. 2014).

We set out to develop a novel reverse phase UHPLC-MS/MS procedure that enable, for a selected ceramide class, the separation, identification and quantification of all individual ceramides. To allow detection of weakly expressed molecules in eleven ceramide classes, we used a scheduled MRM approach for our study. Only ceramides with saturated fatty acids, which are the predominant fatty acid species in ceramides of the skin (Thakoersing et al. 2013), have been investigated.

The goal was to develop methodology for the precise detection of the chain lengths of both, the fatty acid and sphingoid base parts.

## 2 Materials and methods

### 2.1 Chemical

Methanol and Acetonitrile (LC-MS grade, Fisher Chemical, USA), Water (LC-MS Chromasolv, Honeywell, Germany), Tetrahydrofuran (for HPLC, Carlo Erba, Milano, Italy), Dichloromethane (Lichrosolv, Merck Millipore, Billerica, MA, USA) and Formic acid (98–100%, Merck Millipore, Billerica, MA, USA) were used to prepare the lipid samples and mobile phase for UHPLC.

CER[N(C12:0)S(C18)], CER[N(C16:0)S(C18)], CER[N(C17:0)S(C18)], CER[N(C18:0)S(C18)], CER[N(C24:0)S(C18)], CER[N(C16:0)S(C16)], CER[N(C18:0)DS(C18)], CER[N(C24:0)DS(C18)], CER[N(C18:1)DS(C18)], CER[N(C16:0)P(C18)], CER[N(C18:0)P(C18)], CER[N(C24:0)P(C18)], CER[A(C12:0)S(C18)], CER[A(C18:0)S(C18)], CER[A(C22:0)S(C18)], CER[A(C24:0)S(C18)], CER[A(C18:1)S(C18)], CER[A(C24:0)P(C18)], CER[A(C12:0)DS(C18)], CER[A(C16:0)DS(C18)] and CER[A(C18:0)DS(C18)] were bought from Avanti Polar (Alabaster, Alabama, USA), Sigma-Aldrich (St Louis, Missouri, USA) and Cayman chemical (Ann Arbor, Michigan, USA), respectively. CER[E(C18:2)O(C20:0)S(C18)], CER[E(C18:1)O(C20:0)S(C18)], CER[E(C18:2)O(C30:0)S(C18)], CER[E(C18:1)O(C30:0)S(C18)], CER[E(C18:2)O(C20:0)H(C17)] and CER[E(C18:2)O(C30:0)H(C18)] were synthesized by SpiroChem (Zurich, Switzerland).

### 2.2 Collection of *stratum corneum* samples

*Stratum corneum* samples were collected through tape stripping using Dsquames Ø 2.2 cm (Monaderm, Monaco). Three consecutive Dsquames were collected on the lower back.

Each Dsquake was applied multiple times for 1 min until loss of adhesiveness, placed in a bag and stored at  $-18\text{ }^{\circ}\text{C}$ .

### 2.3 Ceramide extraction

Several lipid extraction methods have been tested (Supplemental Table S2) to choose the following optimized method: (a) Three Dsquames were immersed in 3 mL of methanol, vortexed, sonicated for 10 min. and stored at ambient temperature overnight; (b) The methanol fractions were centrifuged at 13,000 RPM during 15 min. using a minispin centrifuge (Eppendorf, Hamburg, Germany); (c) The liquid phase was transferred in a glass tube and methanol was evaporated at  $30\text{ }^{\circ}\text{C}$  under a nitrogen stream; (d) The residue was dissolved in 200  $\mu\text{L}$  dichloromethane/methanol mix (50:50 by vol.) and finally all samples were stored at  $-80\text{ }^{\circ}\text{C}$  until use.

### 2.4 Liquid chromatography and mass spectrometry

Analyses were performed using an Ultimate 3000 RSLC (ThermoScientific, San Jose, CA, USA). Ceramides were separated on an Acquity BEH C8 column ( $150\times 1\text{ mm}$ ,  $1.7\text{ }\mu\text{m}$  particle size; Waters, Milford, MA, USA).

CER[NdS], CER[AdS], CER[NS], CER[AS], CER[NP], CER[AP], CER[NH], and CER[AH] ceramides have been eluted with solvent mixtures of: A (100:0.05 (volume/volume) mixture of water:formic acid); B (100:0.05 (volume/volume) mixture acetonitrile:formic acid). The flow rate was set to 0.1 mL/min, and a gradient with 84% of B to 98% of B over 21.5 min. followed by isocratic elution of 98% B for 8.5 min. was used. The temperature of the column was maintained at  $40\text{ }^{\circ}\text{C}$ . For EO ceramides (CER[EOS], CER[EOH] and CER[EoS]), isocratic elution was performed with the following solvent mix: A, (100:0.05 (volume/volume) mixture of water:formic acid); C (75:25:0.1 (volume/volume) mixture of methanol:tetrahydrofuran:formic acid). The isocratic step was performed with 10% A and 90% C during 20 min. at  $50\text{ }^{\circ}\text{C}$ . The injection volume was 1  $\mu\text{L}$  for both methods.

The RSLC was coupled to a Qtrap 5500 mass spectrometer (Sciex, Concord, Canada) in ESI positive mode, curtain gas (CUR): 30, collision gas (CAD) 200, ion source voltage (IS): 5500 V, source temperature (TEMP):  $400\text{ }^{\circ}\text{C}$ , ion source gas 1 (GS1): 30, ion source gas 2 (GS2): 50, declustering potential (DP): 120 for EOS, EOH and EoS ceramides, for all other ceramides DP was set to 40, enhance potential (EP): 10, collision energy: 45, collision cell exit potential (CXP): 18. MRM parameters for all transitions (precursor and product ions) are listed in the Supplementary Material (Supplemental Table S3). Data analysis and statistical analyses are documented in Supplementary Material.

## 3 Results

The aim of this study was to establish a global profile of non-esterified ceramides (CER[NdS], CER[NS], CER[NP], CER[NH], CER[AdS], CER[AS], CER[AP], CER[AH]) and esterified ceramides (CER[EoS], CER[EOS] and CER[EOH]) of human *stratum corneum*, using a scheduled MRM technique. Firstly, different ceramide classes were separated by UHPLC and determined by their specific retention time. Secondly, the total carbon length of a given ceramide, including both the fatty acid and sphingoid base parts, was calculated based on the molecular mass determined by the precursor ion. Thirdly, the carbon chain length of the sphingoid base was determined via a specific product ion, obtained through fragmentation of the precursor ion. Finally, the carbon chain length of the fatty acid part was deduced from the total carbon number determined in step two via subtraction of the sphingoid base carbon number obtained in step three.

### 3.1 Set up of scheduled-MRM mass spectrometry conditions

To determine the ionization conditions, the mass spectra of ceramide standards have been processed in positive mode, selecting parameters providing the best signal intensities for precursor and product ions. As previously documented, the fragmentation in positive ion mode was dominated by product ions of the sphingoid base chain. Figure 1a shows the fragmentation of dihydroceramide CER[N(C18:0)dS(C18:0)], which resulted in four principal fragments. The first two fragments ( $m/z = 550$  and  $532$ ) were characterized by the successive loss of two water molecules from the precursor ion. The third and fourth ( $m/z = 284$  and  $266$ ) consisted of the sphingoid base part with loss of one and two water molecules, respectively (Gu et al. 1997). The fourth product ion has been selected as MRM transition for ceramide identification and quantification (Table 1). The procedure was validated using chemically synthesized ceramide standards (Supplemental Table S4). Two different Scheduled MRM methods were used; the first for non-esterified ceramides and the second for esterified ceramides (see Sect. 2). Due to the large number of ceramides detected, and the limited acquisition speed of the mass spectrometer for each ceramide class a specific UHPLC run had to be performed.

Figure 1b shows a typical chromatogram for the CER[NS] class (for the list of transitions see Supplemental Table S3). A large degree of complexity was observed and many peaks coeluted. Each group of peaks corresponded to a set of ceramides with the same precursor ion (same

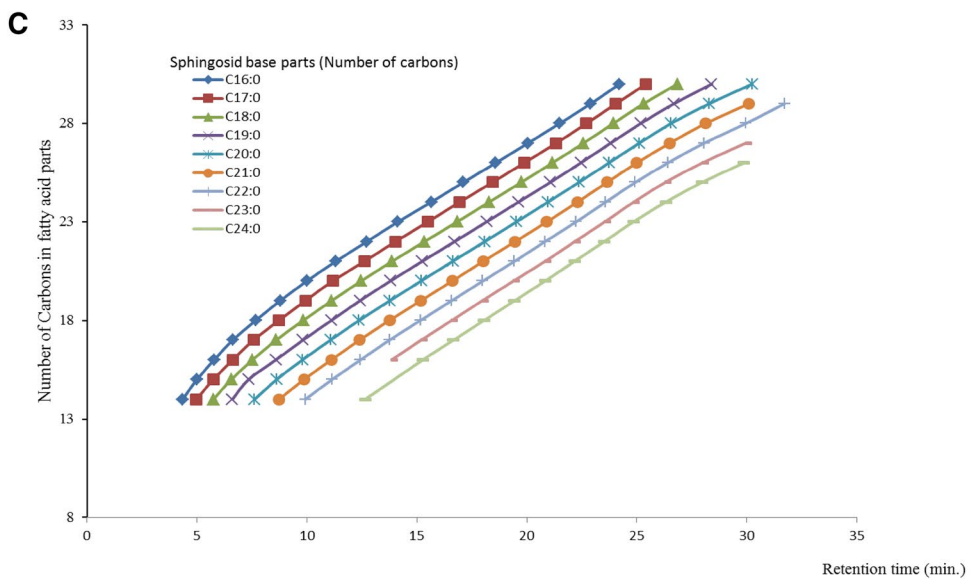
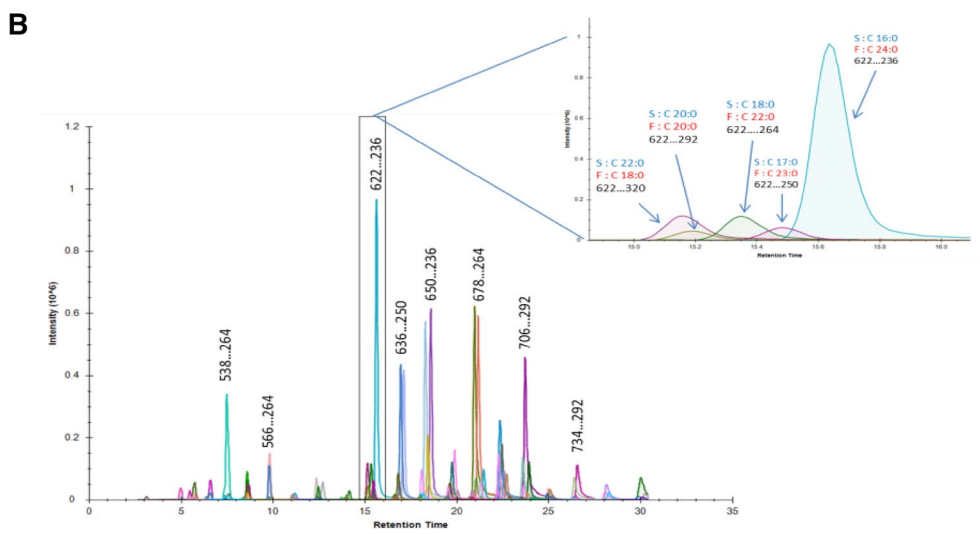
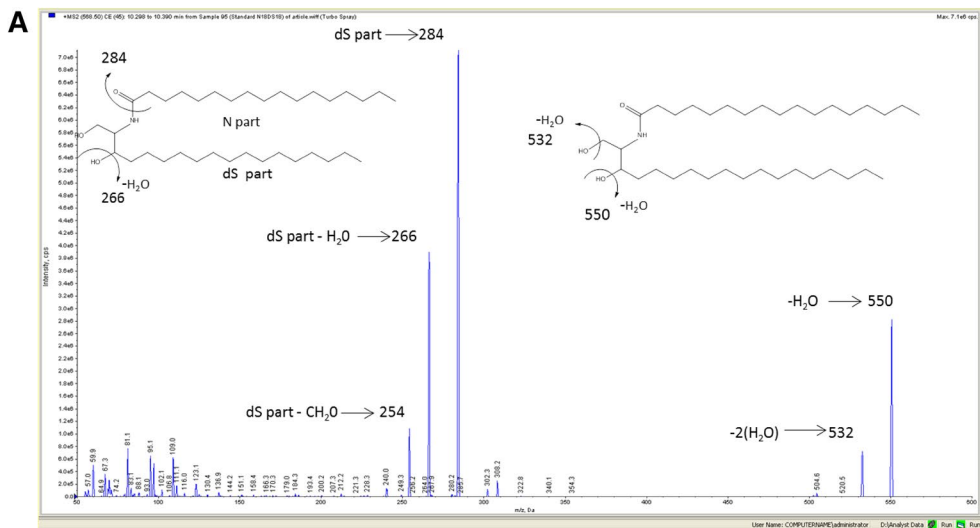


**Fig. 1 a** Positive ESI-MS/MS product ion spectra for ceramide standard CER[NdS] (N C18:0 dS C18:0; m/z 568). Inserts show the molecular structure along with some of the likely fragmentation products. Signal intensities are expressed as counts per second. **b** Extract ion chromatogram of CER[NS] ceramides in positive mode of a healthy human volunteer stratum corneum sample. Zoom shows co-eluting NS ceramides with a length of 40 carbon atoms, which can be distinguished by their respective product ion mass. S, sphingoid base part; F, fatty acid part. **c** Retention times of human NS ceramides for sphingoid base chain lengths of C16:0–C24:0 and fatty acid chain lengths of C14:0–C30:0

total carbon number) (Fig. 1b and Supplemental Fig. S1). A zoom into the retention time zone from 15 to 16 min of the UHPLC chromatogram of the precursor ion 622 m/z, demonstrates the presence of five CER[NS] species corresponding to a total length of 40 carbon atoms. For each of the individual peaks, the product ion compositions were different (number of carbons in sphingoid base and fatty acid parts, respectively). Taking into account the product ion composition, a total of 142 CER[NS] molecules were identified (Fig. 1c).

As all ceramide classes show a common fragmentation pathway (Gu et al. 1997), it has to be noted that, compared to DS sphingoid bases, H sphingoid bases of the same chain length carry an additional oxygen atom (+16 m/z) and an unsaturation (–2 m/z) resulting in a mass difference between the two sphingoid base classes of 14 m/z. This corresponds to the mass of a CH<sub>2</sub> group, therefore, the product ion of a sphingosine H with length n has the same mass as the product ion of the corresponding DS sphingosine with length n + 1 (Table 1) and it is not possible to precisely assign sphingosine H and DS mass spectra to specific molecular structures. To identify individual ceramides of the DS and H class, we therefore developed a UHPLC method allowing the separation of these two ceramide classes.

### 3.2 Optimization of UHPLC conditions for non-esterified and esterified ceramides

Two analytical methods using UHPLC coupled with a Qtrap 5500 mass spectrometer have been developed. The first method, allowing the chromatographic separation of 8 classes of non-esterified ceramides, is based on a linear gradient. For the highly lipophilic CER[EO] class, which eluted too late under these conditions, a second method using isocratic elution with a different solvent mixture was developed (for details refer to Sect. 2).

Figure 2a, b show a subset of the results obtained for the non-esterified ceramides. Data are plotted in two complementary manners. Figure 2a shows the retention times obtained for varying chain length of the fatty acid part (from C12:0 to C30:0) with the chain length of the sphingoid base fixed to C18:0.

Figure 2b presents the alternative curves with the fatty acid set to C18:0, but varying chain lengths in the sphingoid base part (from C16:0 to C25:0).

Retention times combined with the MS/MS data permitted to precisely define the structures of individual ceramides. For example, the curves of the CER[NH] and CER[NDS] classes were clearly separated, allowing for the identification of individual ceramides, even those presenting the same product ion mass (Fig. 2a, b). However, despite the optimization of the UHPLC conditions, ceramides of the CER[NP] and CER [AS] classes coeluted in many circumstances. Again, combining retention times and MS/MS data nevertheless allowed for precisely identifying all detected ceramide molecules. For example, although coeluting at almost the same retention time, CER[N(C18:0)P(C18:0)] and CER[A(C18:0)S(C18:0)] show different precursor and product ions and can be attributed without difficulty (Supplemental Table S3).

Figure 3 demonstrates the results obtained for esterified ceramides of three EO-classes. Using the UHPLC/scheduled-MRM approach described above for non-esterified ceramides, a total of 121 ceramides of the EO-classes, including 50 CER[EOS], 35 CER[EOH] and 36 CER[EODS] species have been separated and identified (for details refer to Sect. 2).

Overall more than 1000 ceramides were identified. Their MS characteristics (precursor and product ion) are provided in Supplemental Table S3.

### 3.3 Relative quantification of CER[AS], CER[NS] and CER[EOS] ceramide expression levels in human and minipig *stratum corneum*

The UHPLC/Scheduled-MRM method was applied to the relative quantification of ceramide expression levels in human and minipig *stratum corneum*. Figures 4 and 5 describe the distribution of individual ceramide species of three ceramide classes, CER[AS], CER[NS] and CER[EOS], observed in *stratum corneum* of healthy human volunteers and minipigs, respectively (for mean, SD and CV values of individual ceramides see Supplemental Table S5). While representatives of all three ceramide classes are found in both human and minipig *stratum corneum*, differences in the relative distribution of specific ceramide species were observed.

Human CER[AS] and CER[NS] typically contain sphingoid bases from 16 to 24 carbon atoms with the 18 carbon sphingoid being the predominant species. Human CER[EOS] forms an exception as the C20:0 sphingoid base is predominant. In minipig, C16:0, C17:0, C18:0 and C20:0 CER[AS] and CER[NS] are most abundant. Within the minipig CER[EOS] class, the C17:0, C18:0 and C20:0 forms are predominant.

**Table 1** Product ions (m/z) selected for the four sphingoid base classes

Length of carbon chain (in sphingoid base part)	Classes of sphingoid bases and product ions selected (m/z)			
	P (Phytosphingosine)	dS (Dihydrosphingosine)	H (6-hydrosphingosine)	S (Sphingosine)
C16:0	254	238	252	236
C17:0	268	252	266	250
C18:0	282	266	280	264
C19:0	296	280	294	278
C20:0	310	294	308	292
C21:0	324	308	322	306
C22:0	338	322	336	320
C23:0	352	336	350	334
C24:0	366	350	Non detected	348
C25:0	Non detected	Non detected	Non detected	362

The masses of the product ions of a 6-hydrosphingosine with length  $C_n$  and of the dihydrosphingosine with length  $C_n + 1$  are identical (color code)

In human, the fatty acid parts of ceramides typically contains from 14 to 30 carbon atoms. Whereas fatty acids with long carbon chains, particularly C24:0 and C26:0 chains are predominant in CER[NS] and for the CER[AS] class C16:0 predominates. Interestingly, the CER[AS] class is distributed in two major blocks. The first is composed of ceramides with fatty acid chain lengths from 16 to 18 carbon atoms, and the second of ceramides with fatty acid chain lengths from 24 to 26 carbon atoms. In CER[EOS], the 30 carbon linker largely predominates. In minipig, the C16:0 fatty acid CER[AS] is predominant and one does not observe a clear separation in two blocks. In the CER[NS] class the fatty acid distributions are more homogeneous with, however, less abundant odd number carbon chains. In minipig CER[EOS], different to the observations in human, the C28:0 linker is strongly abundant in addition to C30:0.

In human, for all three ceramide classes CER[AS], CER[NS] and CER[EOS], for both the sphingoid base and the fatty acid parts, even chain species are about twofold more abundant (Supplemental Fig. S2). Similar findings were observed in minipigs. Within the odd sphingoid bases, the 17 carbon chain is the most prevalent (Fig. 5) (t'Kindt et al. 2012).

## 4 Discussion

Based on the non-invasive collection of 3 Dsquames, only, we developed a new large scale analytical method for the comprehensive analysis of ceramides in *stratum corneum*. Two UHPLC conditions running for 30 min, one using a gradient and the second an isocratic elution system, respectively, permitted the analysis of all individual ceramide species belonging to 11 ceramide classes. Analysis of the

twelfth class (CER[EOP]) is in progress. Although only a small number of synthetic ceramide standards were available, the curves resulting from the correlation between total carbon chain length and retention time provided the necessary precision to establish a robust method.

Based on a scheduled-MRM library containing the precursor and product ions, as well as the associated retention times, a dictionary of individual ceramide species has been established. Scheduled MRM transitions of the targeted analytes are monitored only around the expected retention time. Thus, automated MRM scheduling decreases the number of concurrent MRM transitions, allowing both the cycle time and the dwell time to be optimized for highest sensitivity, accuracy, and reproducibility. In effect, scheduled MRM monitors many more MRM transitions in a single acquisition speeding up the analysis without compromising data quality. The method therefore is characterized by high sensitivity and specificity. More than 1000 individual ceramide species have been identified and semi-quantified resulting in the most comprehensive description of individual ceramide species reported to date, more than doubling the number of previously described ceramides (Boiten et al. 2016; Jia et al. 2016; t'Kindt et al. 2012). Furthermore, the large scale description of individual ceramide species with precisely determined fatty acid- (or linker-) and sphingoid parts, respectively, is novel.

Using the newly developed method and a cohort of ten healthy human volunteers, comprehensive ceramide profiling was performed for three classes, CER[AS], CER[NS] and CER[EOS]. Our study confirms the high diversity in fatty acid and sphingoid base lengths of individual ceramide species (Jeroen van Smeden and Bouwstra 2016; van Smeden et al. 2014). For all 11 ceramide classes studied, and in agreement with the literature (Farwanah et al. 2007;

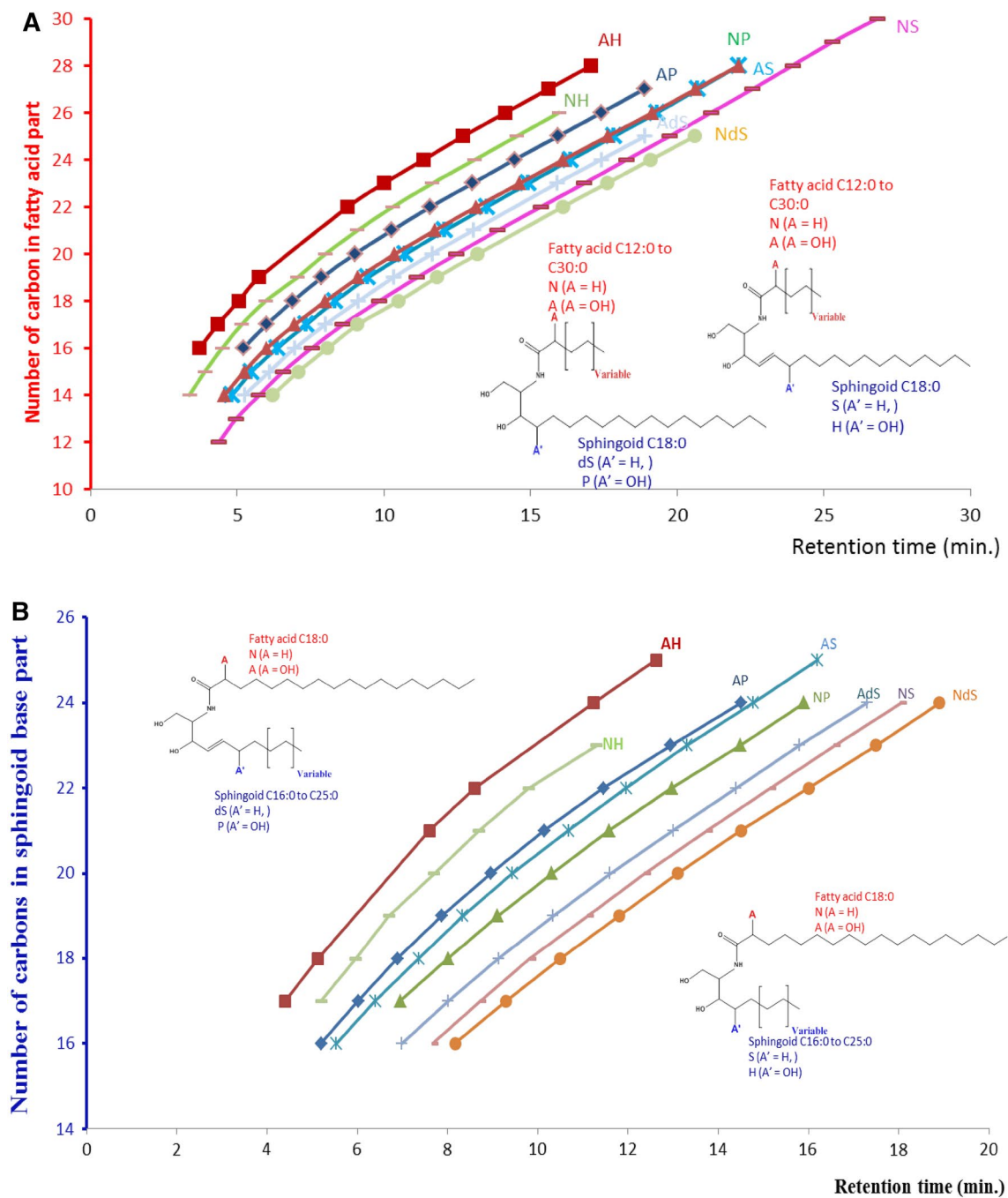


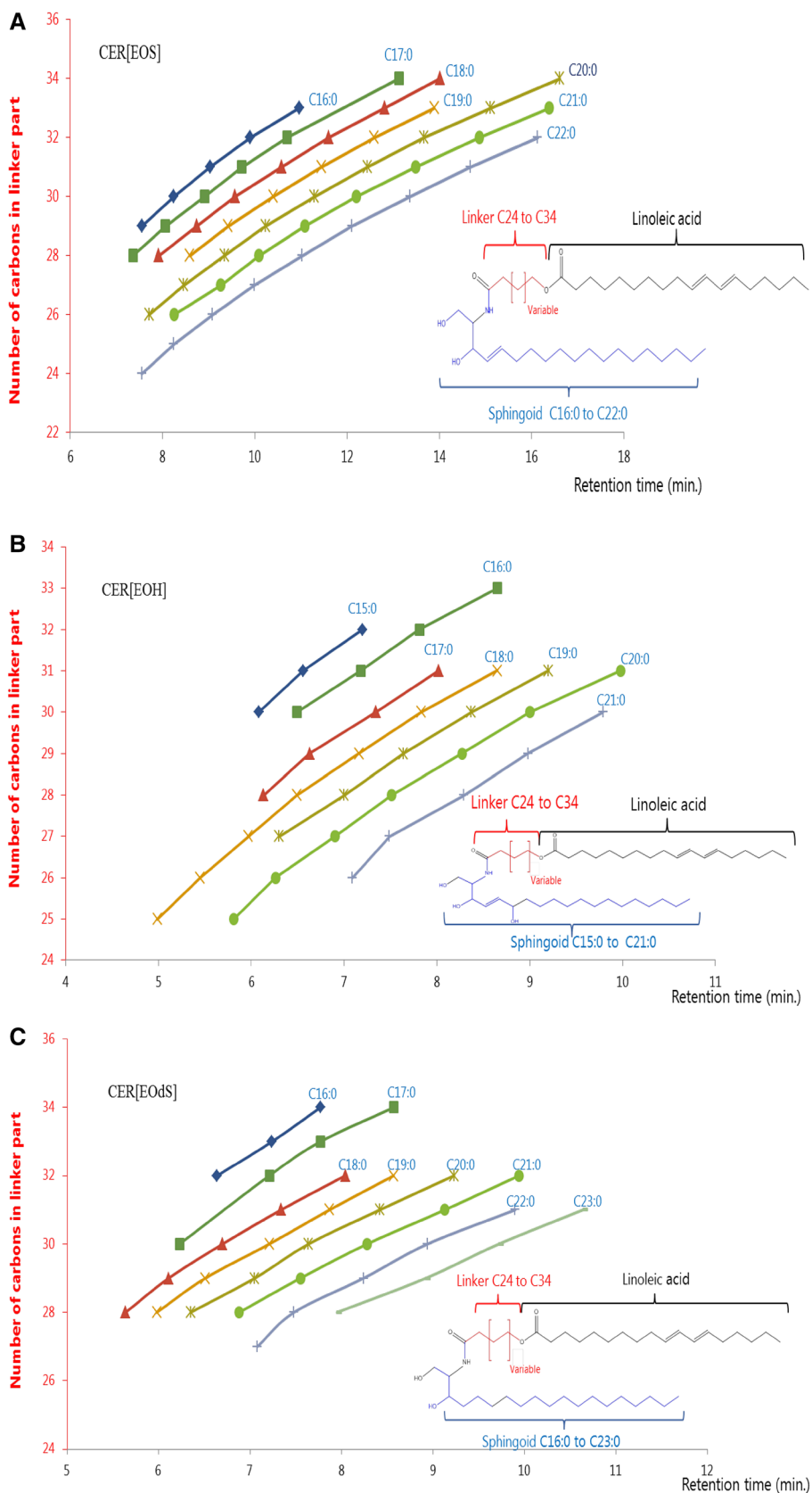
**Fig. 2 a** Retention times of human non-esterified ceramide classes CER[NS], [AS], [NH], [NP], [AP], [AH], [NdS] and [AdS]. Sphingoid base chain length fixed to C18:0, fatty acid chain lengths from C12:0 to C30:0. Inserts show the molecular structures of the studied ceramides. **b** Retention times of human non-esterified ceramide

classes CER[NS], [AS], [NH], [NP], [AP], [AH], [NdS] and [AdS]. Sphingoid base chain length from C16:0 to C25:0, fatty acid chain length fixed to C18:0. Inserts show the molecular structures of studied ceramides

Jenkins et al. 2015; t'Kindt et al. 2012), ceramides with an odd number of carbon atoms were observed at lower abundance, than ceramides with an even number of carbon atoms. Human fatty acid metabolism mainly produces even chain fatty acids with a carbon chain length of 2–26. These fatty

acids represent > 99% of the total fatty acids that can be found in human plasma. Only four significantly measurable odd chain fatty acids (C15:0, C17:0, C17:1 and C23:0) were detected in human plasma (Jenkins et al. 2015; Nagy et al. 2013), leading to the conclusion that odd chain free

**Fig. 3** Retention times of human esterified ceramide classes CER[EOS], CER[EOH] and CER[EoS]. Sphingoid base part from C16:0 to C23:0. Linker part from C24:0 to C34:0. Inserts show the molecular structures of studied ceramides





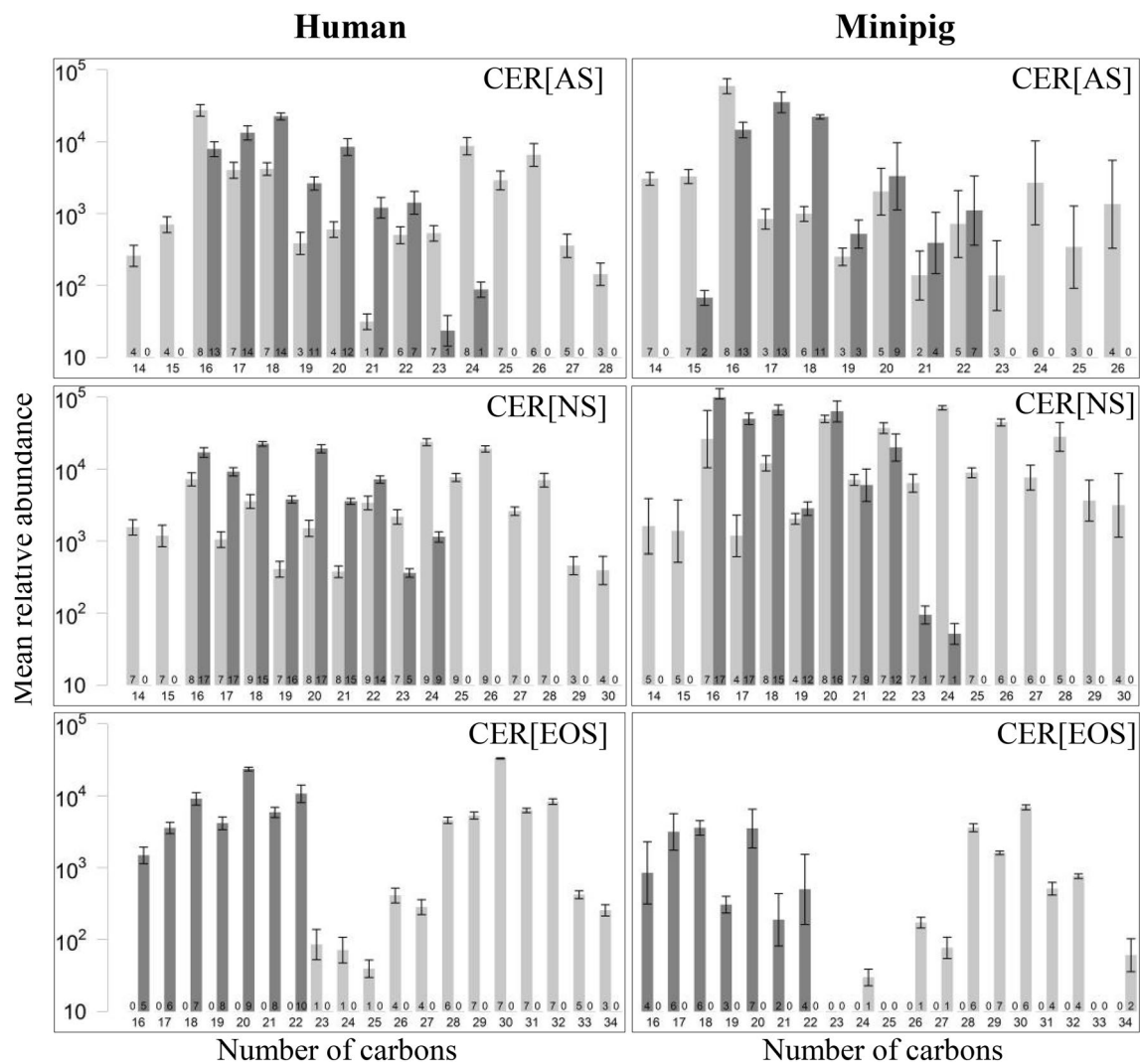


**Fig. 4** Mean relative abundance of fatty acid- (linker- for CER[EOS]) (grey bars) and sphingoid base (black bars) parts among ten healthy volunteers (left) and five minipigs (right) for CER[AS], CER[NS] and CER[EOS]. Ceramides are ordered by total carbon length (x-axis).

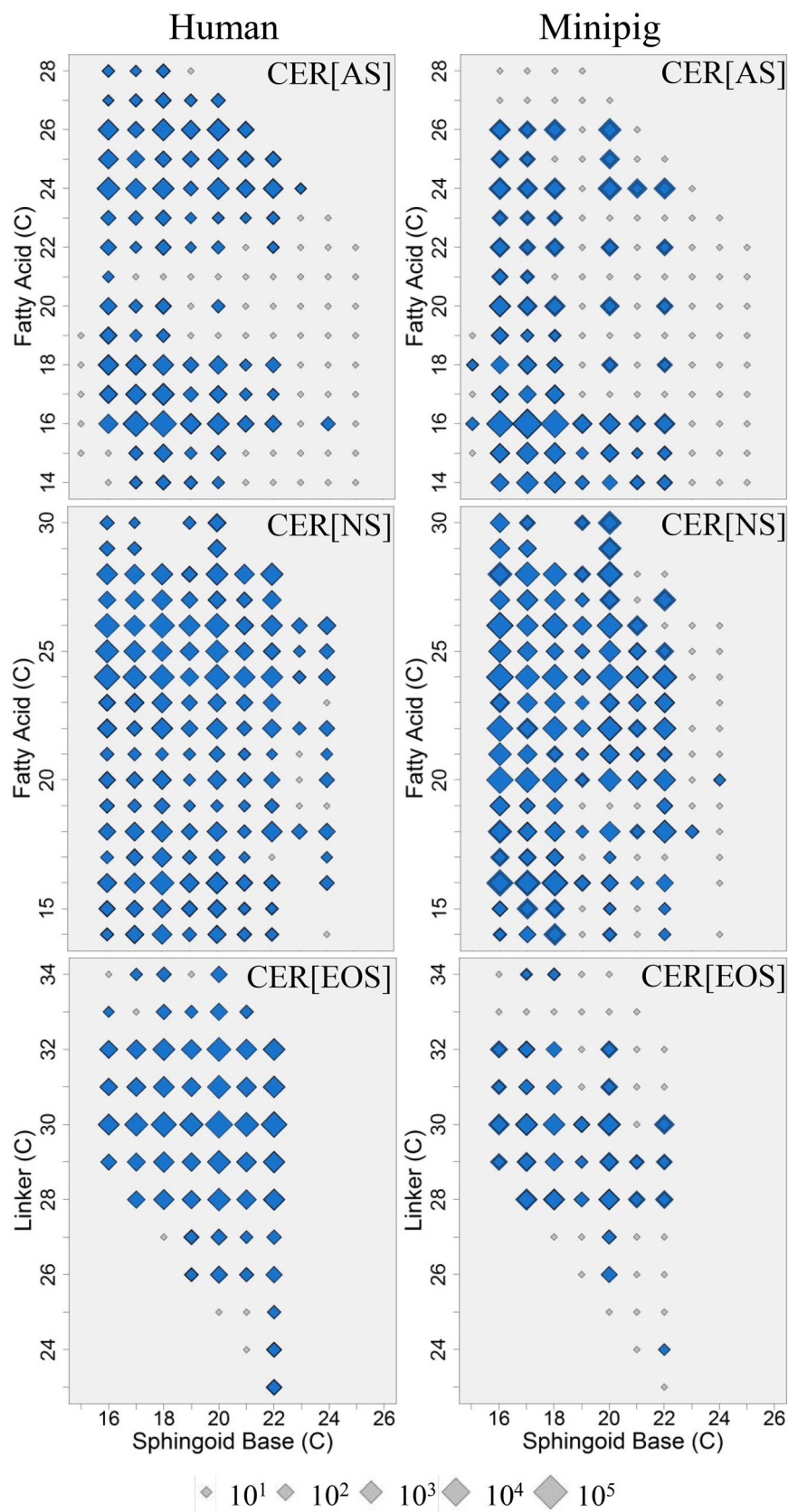
Standard deviations are indicated as error bars. Numbers included within each individual bar represent the number of quantifiable ceramides

fatty acids play a minor physiological role in plasma (Schulz 2002). In contrast to plasma, and in line with the results of this study, a relatively high content of odd chain fatty acids and sphingoid bases was found in human skin (Jenkins et al. 2015). While the presence of odd chain fatty acids is generally attributed to dietary intake, the reason for this striking difference seems to be poorly understood (Jenkins et al. 2015).

Generally, whereas sphingoid bases with a chain length of C16–C20 are most abundant, fatty acid parts with long chains of > 24 carbons predominate. This observation can be linked to the substrate specificity of the enzymes involved in ceramide synthesis. Although also accepting slightly shorter and longer fatty acyl-CoA molecules, serine palmitoyl transferase (STP) involved in

the condensation of L-serine with fatty acyl-CoA, predominantly generates C18 sphingoid bases (Rabionet et al. 2014). In mammals, six ceramide synthases (CerS1 to CerS6) have been identified. These demonstrate different substrate specificities: CerS5 and CerS6 prefer C16-CoA, whereas CerS1 prefers C18-CoA. CerS2 has high affinity for very long chain fatty acids ranging from C20:0 to C26:0. (Rabionet et al. 2014). CerS3 was identified to be exclusively required for ultra-long-chain acyl moieties ( $\geq$  C26:0) in vitro and in vivo (Jennemann et al. 2012; Rabionet et al. 2014). CerS3 knockout mice demonstrate severe skin barrier defects accompanied by a deficiency in epidermal keratinization and a strong increase in transepidermal water loss, ultimately leading to death (Eckl et al. 2013; Farwanah et al. 2007).

**Fig. 5** Mean normalized relative abundances of individual ceramides among ten healthy volunteers (left) and five minipigs (right) for CER[AS], CER[NS] and CER[EOS] are shown. The standard deviation is indicated by superposed diamonds. The ceramides are ordered and detailed by the number of carbon atoms for the sphingoid base (x-axis) and the fatty acid or linker-part (y-axis). Within a given ceramide class, blue diamonds correspond to ceramides identified in >70% of samples. Grey diamonds correspond to ceramides identified in <70% of samples. Empty positions depict ceramide species that although screened for, have not been observed. The size of the diamonds indicates the relative abundance (see legend on bottom of the figure)



The close anatomical, biochemical and physiological similarities of porcine skin with human skin make the minipig a favorable non-rodent species in the efficacy and safety assessment of dermal topical products. Pig skin is also used routinely for PK studies (Mahl et al. 2006; Svendsen 2006; Weaver et al. 2016). It is, therefore, of strong interest to understand the similarities and differences between human and pig skin with respect to key epidermal barrier lipids as these affect the penetration and absorption of test substances. CER[AS], CER[NS] and CER[EOS] have been analyzed in minipig *stratum corneum*. Overall, the same ceramide species were identified in human and minipig, with some alterations in relative composition. Most surprising was the strong abundance in minipig of the CER[AS] sphingoid base C17:0. It should be noted, however, that this sphingoid base was also the most prominent odd chain sphingoid base in human ceramides. Functional studies will be necessary to decipher if the observed differences in ceramide composition impact the pig skin barrier and if this results in significantly altered penetration of exogenously applied molecules, compared to human skin. Anatomical factors like the very different hair follicle and subcutaneous fat structures might impact penetration of exogenously applied molecules even more strongly.

In summary, the novel UHPLC/Scheduled MRM method combined with non-invasive *stratum corneum* sampling permitted the identification and relative quantification of > 1000 ceramide species in eleven ceramide classes, and the comparison of the ceramide composition of human and pig *stratum corneum*. In the future the methodology will be applied for the analysis of epidermal ceramide distribution across species in healthy as well as pathological skin. Finally, the precise identification and relative quantification of a large number of individual ceramide molecules will allow for reliable biomarker studies in preclinical and clinical settings.

**Acknowledgements** The authors are grateful to Charbel Azar and Thierry Alvarez for the collection of minipig *stratum corneum* samples, to Oana Hulea and Malthide Moyne for the development of UPLC methods, and to Paul Fogel and Michel Poncet for statistical assistance.

**Author contributions** GPL, VA and AG performed all sample analysis. Data analysis and interpretation was carried out in collaboration between GPL, BG and JJV. GPL and JJV wrote the manuscript together. All authors have participated in critical data interpretation and acceptance of the manuscript.

## Compliance with ethical standards

**Conflict of interest** The authors declare that they have no conflict of interest and no conflict of financial interest.

**Ethical approval** The work was performed in accordance with the code of ethics of the world medical association (Declaration of Helsinki). Informed consent was obtained for all 10 healthy volunteers enrolled

in the study. The study was approved by the local ethics committee (CPP Sud-Méditerranée V, Hôpital de Cimiez, NICE, France). For Göttingen minipigs, an equivalent sampling process was performed on the flank of 5 animals. All animal experiments were compliant with the EU Directive 2010/63/EU.

## References

- Boiten, W., Absalah, S., Vreeken, R., Bouwstra, J., & van Smeden, J. (2016). Quantitative analysis of ceramides using a novel lipidomics approach with three dimensional response modelling. *Biochimica et Biophysica Acta*, 1861(11), 1652–1661. <https://doi.org/10.1016/j.bbali.2016.07.004>.
- Eckl, K. M., Tidhar, R., Thiele, H., Oji, V., Hausser, I., Brodesser, S., et al. (2013). Impaired epidermal ceramide synthesis causes autosomal recessive congenital ichthyosis and reveals the importance of ceramide acyl chain length. *Journal of Investigative Dermatology*, 133(9), 2202–2211. <https://doi.org/10.1038/jid.2013.153>.
- Elias, P. M. (2014). Lipid abnormalities and lipid-based repair strategies in atopic dermatitis. *Biochimica et Biophysica Acta*, 1841(3), 323–330. <https://doi.org/10.1016/j.bbali.2013.10.001>.
- Farwanah, H., Pierstorff, B., Schmelzer, C. E. H., Raith, K., Neubert, R. H. H., Kolter, T., et al. (2007). Separation and mass spectrometric characterization of covalently bound skin ceramides using LC/APCI-MS and Nano-ESI-MS/MS. *Journal of Chromatography B*, 852(1), 562–570. <https://doi.org/10.1016/j.jchromb.2007.02.030>.
- Feingold, K. R., & Elias, P. M. (2014). Role of lipids in the formation and maintenance of the cutaneous permeability barrier. *Biochimica et Biophysica Acta (BBA) - Molecular and Cell Biology of Lipids*, 1841(3), 280–294. <https://doi.org/10.1016/j.bbali.2013.11.007>.
- Grösch, S., Schiffmann, S., & Geisslinger, G. (2012). Chain length-specific properties of ceramides. *Progress in Lipid Research*, 51(1), 50–62. <https://doi.org/10.1016/j.plipres.2011.11.001>.
- Gu, M., Kerwin, J. L., Watts, J. D., & Aebersold, R. (1997). Ceramide profiling of complex lipid mixtures by electrospray ionization mass spectrometry. *Analytical Biochemistry*, 244(2), 347–356. <https://doi.org/10.1006/abio.1996.9915>.
- Hinder, A., Schmelzer, C. E., Rawlings, A. V., & Neubert, R. H. (2011). Investigation of the molecular structure of the human *stratum corneum* ceramides [NP] and [EOS] by mass spectrometry. *Skin Pharmacology and Physiology*, 24(3), 127–135. <https://doi.org/10.1159/000322303>.
- Imokawa, G., Abe, A., Jin, K., Higaki, Y., Kawashima, M., & Hidano, A. (1991). Decreased level of ceramides in *stratum corneum* of atopic dermatitis: An etiologic factor in atopic dry skin? *Journal of Investigative Dermatology*, 96(4), 523–526. <https://doi.org/10.1111/1523-1747.ep12470233>.
- Janssens, M., van Smeden, J., Gooris, G. S., Bras, W., Portale, G., Caspers, P. J., et al. (2012). Increase in short-chain ceramides correlates with an altered lipid organization and decreased barrier function in atopic eczema patients. *Journal of Lipid Research*, 53(12), 2755–2766. <https://doi.org/10.1194/jlr.P030338>.
- Jenkins, B., West, J. A., & Koulman, A. (2015). A review of odd-chain fatty acid metabolism and the role of pentadecanoic acid (c15:0) and heptadecanoic acid (c17:0) in health and disease. *Molecules*, 20(2), 2425–2444. <https://doi.org/10.3390/molecules20022425>.
- Jennemann, R., Rabionet, M., Gorgas, K., Epstein, S., Dalpke, A., Rothermel, U., et al. (2012). Loss of ceramide synthase 3 causes lethal skin barrier disruption. *Human Molecular Genetics*, 21(3), 586–608. <https://doi.org/10.1093/hmg/ddr494>.
- Jia, Z. X., Zhang, J. L., Shen, C. P., & Ma, L. (2016). Profile and quantification of human *stratum corneum* ceramides by normal-phase

- liquid chromatography coupled with dynamic multiple reaction monitoring of mass spectrometry: Development of targeted lipidomic method and application to human stratum corneum of different age groups. *Analytical and Bioanalytical Chemistry*, 408(24), 6623–6636. <https://doi.org/10.1007/s00216-016-9775-6>.
- Jungersted, J. M., Hellgren, L. I., Jemec, G. B. E., & Agner, T. (2008). Lipids and skin barrier function: A clinical perspective. *Contact Dermatitis*, 58(5), 255–262. <https://doi.org/10.1111/j.1600-0536.2008.01320.x>.
- Kezic, S., Novak, N., Jakasa, I., Jungersted, J. M., Simon, M., Brandner, J. M., et al. (2014). Skin barrier in atopic dermatitis. *Frontiers in Bioscience (Landmark Edition)*, 19, 542–556. <https://doi.org/10.2741/4225>.
- Mahl, J. A., Vogel, B. E., Court, M., Kolopp, M., Roman, D., & Nogues, V. (2006). The minipig in dermatotoxicology: Methods and challenges. *Experimental and Toxicologic Pathology*, 57(5–6), 341–345. <https://doi.org/10.1016/j.etp.2006.03.004>.
- Masukawa, Y., Narita, H., Sato, H., Naoe, A., Kondo, N., Sugai, Y., et al. (2009). Comprehensive quantification of ceramide species in human stratum corneum. *Journal of Lipid Research*, 50(8), 1708–1719. <https://doi.org/10.1194/jlr.D800055-JLR200>.
- Nagy, K., Sandoz, L., Destaillets, F., & Schafer, O. (2013). Mapping the regioisomeric distribution of fatty acids in triacylglycerols by hybrid mass spectrometry. *Journal of Lipid Research*, 54(1), 290–305. <https://doi.org/10.1194/jlr.D031484>.
- Pilgram, G. S. K., Vissers, D. C. J., van der Meulen, H., Koerten, H. K., Pavel, S., Lavrijsen, S. P. M., et al. (2001). Aberrant lipid organization in stratum corneum of patients with atopic dermatitis and lamellar ichthyosis. *Journal of Investigative Dermatology*, 117(3), 710–717. <https://doi.org/10.1046/j.0022-202x.2001.01455.x>.
- Rabionet, M., Bayerle, A., Marsching, C., Jennemann, R., Gröne, H.-J., Yildiz, Y., et al. (2013). 1-O-acylceramides are natural components of human and mouse epidermis. *Journal of Lipid Research*, 54(12), 3312–3321.
- Rabionet, M., Gorgas, K., & Sandhoff, R. (2014). Ceramide synthesis in the epidermis. *Biochimica et Biophysica Acta*, 1841(3), 422–434. <https://doi.org/10.1016/j.bbalip.2013.08.011>.
- Schulz, H. (2002). Chapter 5 oxidation of fatty acids in eukaryotes. *New Comprehensive Biochemistry*, 36, 127–150.
- Svendsen, O. (2006). The minipig in toxicology. *Experimental and Toxicologic Pathology*, 57(5–6), 335–339. <https://doi.org/10.1016/j.etp.2006.03.003>.
- t'Kindt, R., Jorge, L., Dumont, E., Couturon, P., David, F., Sandra, P., et al. (2012). Profiling and characterizing skin ceramides using reversed-phase liquid chromatography–quadrupole time-of-flight mass spectrometry. *Analytical Chemistry*, 84(1), 403–411. <https://doi.org/10.1021/ac202646v>.
- Thakoersing, V. S., van Smeden, J., Mulder, A. A., Vreeken, R. J., Ghalbzouri, A., & Bouwstra, J. A. (2013). Increased presence of monounsaturated fatty acids in the stratum corneum of human skin equivalents. *Journal of Investigative Dermatology*, 133(1), 59–67. <https://doi.org/10.1038/jid.2012.262>.
- van Smeden, J., & Bouwstra, J. A. (2016). Stratum corneum lipids: Their role for the skin barrier function in healthy subjects and atopic dermatitis patients. In *Skin barrier function* (Vol. 49, pp. 8–26). Basel: Karger Publishers.
- van Smeden, J., Janssens, M., Gooris, G. S., & Bouwstra, J. A. (2014). The important role of stratum corneum lipids for the cutaneous barrier function. *Biochimica et Biophysica Acta (BBA) - Molecular and Cell Biology of Lipids*, 1841(3), 295–313. <https://doi.org/10.1016/j.bbalip.2013.11.006>.
- Vietzke, J.-P., Brandt, O., Abeck, D., Rapp, C., Strassner, M., Schreiner, V., et al. (2001). Comparative investigation of human stratum corneum ceramides. *Lipids*, 36(3), 299–304. <https://doi.org/10.1007/s11745-001-0721-9>.
- Weaver, M. L., Grossi, A. B., Schutzack, J., Parish, J., Logsted, J., Bogh, I. B., et al. (2016). Vehicle systems and excipients used in minipig drug development studies. *Toxicologic Pathology*, 44(3), 367–372. <https://doi.org/10.1177/0192623315613088>.